Boundary Layer Meteorology manuscript No.
(will be inserted by the editor)

The growth of the planetary boundary-layer at a coastal site: a case study

Ferdinando De Tomasi · Vincenzo Bellantone · M. Marcello Miglietta · M. Rita Perrone

December 15, 2010

Abstract A lidar system is used to determine the diurnal evolution of the planetary boundary-layer (PBL) height on a summer day characterised by anticyclonic conditions. The site is located on a peninsular some 15 km distant from the sea in south-east Italy. Contrary to expectations, the PBL height, after an initial growth consequent to sunrise, ceases to increase about two hours before noon and then decreases and stabilises in the afternoon. The interpretation for such an anomalous behaviour is provided in terms of trajectories of air parcels towards the lidar site, which are influenced by the sea breeze, leading to a transition from a continental boundary-layer to a coastal internal boundary-layer. The results are analysed using mesoscale numerical model simulations and a simple model that allows for a more direct interpretation of experimental results.

Keywords Aerosol, Lidar, Planetary boundary-layer modelling, Sea breeze

PACS 92.60.Fm, 92.60.Gn

1 Introduction

Understanding the characteristics of the diurnal evolution of the planetary boundary-layer (PBL) height is important for several reasons, such as the assessment of air quality, meteorological forecasts and climate studies. The main characteristics are well understood and described in e.g. Garratt (1992),

F. De Tomasi, V.Bellantone, M.R. Perrone
Dipartimento di Fisica, Universitá del Salento, via Arnesano I-73100 Lecce, Italy.
E-mail: Ferdinando.DeTomasi@unisalento.it

M.M Miglietta
CNR- Istituto per lo Studio dell'Atmosfera e del Clima (ISAC), corso Stati Uniti, Padova,Italy

Stull (1988). In anticyclonic conditions, the PBL height over land usually commences growth from about one hour after sunrise, when an effective heating of the soil takes place, then stabilises around noon. Such evolution can be monitored in real time using remote sensing systems such as lidar, sodar, microwave wind profiler (Seibert et al., 2000). The direct measurements of the PBL height can nowadays be considered a common and relatively simple task: as an example, the purpose of the "High Resolution Boundary Layer Analysis Project"from NOAA-NASA-NCAS is aimed at the real-time monitoring of the PBL over the USA using all available data (McQueen et al., 2010). The meteorological services of several European countries (United Kingdom, Germany, The Netherlands, France, Finland) mantain networks of ceilometers for PBL profiling (Wauben et al., 2008; Haeffelin et al., 2009). These instruments are however relatively expensive; as a result there is not yet in place an operational global network for PBL height, apart from the indirect measurements from radiosoundings, which, however, are sparse in time and space. It is not uncommon that large regions, even in developed countries, are devoid of boundary-layer measurements. So, the need for estimating the PBL height from ground parameters that are simple to measure, although less important than in the past, is still relevant. Such estimations could be used for comparison and interpolation of the existing measurements and simulations.

In the case of homogeneous terrain, the growth of the PBL can be predicted from measurements of the heat and momentum fluxes at the surface, using an appropriate parametrisation, and an ordinary differential equation is usually sufficient to describe the PBL cycle (Carson, 1973; Tennekes, 1973; Batchvarova and Gryning, 1991). In the case of inhomogeneous terrain, more complicated phenomena occur because the PBL height now depends on the history of the air parcels. The most important feature is the internal boundary-layer (IBL), and in the case of onshore flows, the IBL height increases inland from the coast. In general, the description of the IBL requires measurements at different points of the coastal region, because the equilibrium height is reached after several kilometres fetch. Field campaigns usually need a network of remote sensing measurements or mobile instruments.

A review of measurements and models of IBL is given by Garratt (1990). As examples of more recent field campaigns, we cite studies in Athens (Melas and Kambezidis, 1992), the PACIFIC93 experiment in Canada (Steyn et al., 1997), fumigation studies in Australia (Luhar et al., 1998). From the experimental point of view, lidars on board of aircraft allow the monitoring of the spatial variation of the internal boundary-layer (McElroy et al., 1991; McCormick, 2005).

Compared to the homogeneous terrain case, more sophisticated models are needed because the spatial variation of the PBL height and other relevant parameters must be taken into account. In the following, we refer to one-dimensional (1D), two-dimensional (2D), three-dimensional (3D) models to indicate the number of spatial dimensions that, besides time variations, are considered.

Most of the emphasis in the past has been given to the case of one spatial dimension, which is usually sufficient when small fetches are considered, and to the spatial growth of the internal boundary-layer. A steady-state solution has been given by Gryning and Batchvarova (1990) and a generalisation has been given by Luhar (1998). A comparison of different models with observations obtained in Athens has been given by Melas and Kambezidis (1992), who showed that the best performances are obtained by the model of Gryning and Batchvarova (1990).

The spatial-temporal description of the IBL is complicated by the fact that, close to the coast and in fair weather conditions, the sea breeze is present (Abbs and Physick, 1992; Simpson, 1994; Miller et al., 2003). In the case of weak synoptic forcing, the sea breeze induces a circulation in which, in the lower onshore part, an internal boundary-layer is formed, and in the upper part a return flow towards the sea is observed. This process leads to a layering of the aerosol load that can be observed by lidar. When a synoptic forcing is present, the sea breeze enforces the synoptic wind and changes its direction; it is possible that, in this case, no return flow exists. In conclusion, we can say that changing winds are often observed close to the coasts, so that stationary approximations could not be suited to the description of the internal boundary-layer.

In cases of irregular coastline or a complex terrain, full mesoscale models (Melas et al., 1995) or generalisations of the 1D PBL models accounting for the 2D spatial variations can be used (Gryning and Batchvarova, 1996). Such models consider both space and time evolution and it has been shown that they compare well with measurements and mesoscale model results (Batchvarova et al., 1999).

Many studies have dealt with the evolution of the boundary-layer in coastal sites, and its interaction with the sea breeze. However, few address the problem of its diurnal evolution (Martano, 2002; Talbot et al., 2007); most of the available studies in the Mediterranean Sea are concentrated in large agglomerations such as Athens (Melas and Kambezidis, 1992; Batchvarova and Gryning, 1998), Barcelona (Sicard et al., 2006), Marseille (Delbarre et al., 2005; Lemonsu et al., 2006), Naples (Boselli et al., 2009), Rome (Mastrantonio et al., 1994), Thessaloniki (Santacesaria et al., 1998). In such cases the presence of the city and a complex orography complicate the analysis.

The characteristics of the boundary-layer are also important to understand the properties of atmospheric aerosols. Because of the short lifetime of the aerosol, they present an extreme spatial-temporal variability, and their concentration will depend on the characteristics of the planetary boundary-layer. Thus, an interpretation of aerosols measurements needs concomitant PBL properties measurements, and, for this reason, the recently implemented networks for measurements of aerosol load require PBL height measurements. For example, the European network EARLINET (Bösenberg et al., 2003), composed of several lidar stations spread in the whole Europe, measures the altitude resolved optical properties of aerosol (backscattering and extinction) three times per week. The present authors mantain a station of the network

at Lecce, in south-east Italy. The PBL height can be inferred from lidar signals (as will be explained in the following), and then this variable is reported, for each station, in the data base of the network. A report of the first phase of the project (2000-2002), in which the PBL height climatology is reported for 10 stations, has been published in Matthias et al. (2004). They show that the PBL height evolution throughout the year has an anomalous behaviour at the Lecce site in comparison to all of the other EARLINET stations. In general, it is expected that the PBL height follows a seasonal cycle with a maximum in summer, mainly because of the larger soil temperature, and as a consequence, larger heat and momentum fluxes during summer. However, at the Lecce site, an inverted cycle is found. This result is consistent with the analysis of Dayan et al. (1996), based on the available radiosoundings in the Mediterranean basin; this behaviour has been interpreted by analysing the seasonal synoptic situation. We have analysed in detail the PBL heights from the lidar measurements in Lecce (De Tomasi and Perrone, 2006) and compared them with PBL heights as determined from vertical profiles at a radiosounding station close to Lecce (Brindisi). Both techniques display in average the same behaviour, but the comparison of single measurements suggests that the sea breeze influences the development of the boundary-layer.

Here, we present a case study in which the means by which the sea breeze influences the growth of the PBL inland is shown clearly. It is shown, from a detailed analysis of one case of PBL growth in a simple-orography coastal site, that the PBL height can actually decrease when the solar irradiation is maximum, contrary to what is expected. The high temporal and vertical resolution monitoring with lidar shows details that, even if already observed (Steyn and Oke, 1982; Batchvarova and Gryning, 1998; Batchvarova et al., 1999; Puygrenier et al., 2005), have received little attention to date.

The paper is organized as follows: in Section 2 the lidar site and the surrounding region are described, together with the relevant climatological information. Then, we briefly describe the experimental apparatus and the techniques for the PBL height determination in Section 3. PBL heights inferred from lidar and ancillary measurements are described in Section 4. A mesoscale simulation using a numerical model is described in Section 5. Finally, a simple model for the PBL growth based on local measurements is used to reproduce experimental results (Section 6).

2 Description of the site

The lidar site is located at the Physics Department of Università del Salento (40.33 N, 18.11 E), in the neighbourhood of Lecce, Italy, at an altitude of 30 m a.s.l. Figure 1a, reproducing the Salento peninsula, shows that the site is 15 km far from the Adriatic sea and 20 km from the Ionian sea. The region is flat and the environment is mostly rural (grapes and olive tree cultivations); however, a high density of small towns is present. In summer, anticyclonic conditions generally affect the central and western Mediterranean Sea, due to

the northward extension of the Azores high. As a consequence, the dominant synoptic wind on the Adriatic coast is northerly and its intensity can be locally enhanced by the orography and thermal phenomena. However, when the northerly synoptic component is weak, the sea breeze on the Ionian side of the peninsula can offset the synoptic component and produce southerly winds on the Ionian coast. In this case, convergence with the Adriatic breeze circulation may occur (Mangia et al., 2004), but the extent of the Ionian breeze is generally confined to a small area and does not affect the lidar site. Actually, we observe that the wind observed at the lidar site is correlated with the wind observed on the close Adriatic coast, even though no systematic measurement exists. Furthermore, it must be stated that, in the surroundings of the lidar site, the Adriatic coastline is almost entirely characterized by sand beaches; thus, as a first approximation, the complexity of the terrain can be reduced to the transition between sea and land and the situation is close to an ideal, straight shoreline.

Based on the map in Fig. 1 we can see that, if the wind is oriented along the peninsula axis (300°), the air parcels arriving to the lidar site have travelled essentially over land. Conversely, if the wind is oriented from north-east (around 45°), the air parcels come from the sea and travel on the land only for a few kilometres. Between these two extremes, there are intermediate situations that depend on the exact configuration of the wind field and thus the properties of the boundary-layer will be consequently affected. We can estimate, as an example, the order of magnitude of this effect by calculating the time spent over land by an air parcel arriving from the sea to the lidar site following a straight line at a constant speed of 5 m s^{-1}. In Fig. 1b this time is reported as a function of the wind direction showing that it can vary from several hours to less than an hour. Very different effects on the growth of the boundary-layer are thus expected, because in the first case we will deal with a continental boundary-layer, while in the last case an internal boundary-layer will be observed.

3 The experimental apparatus and measurement techniques

The lidar system has been described in detail by De Tomasi and Perrone (2003). It is based on a XeF excimer laser emitting at 351 nm. Though the system is a Raman lidar that can directly measure the aerosol extinction and the water vapour mixing ratio, these possibilities are limited to nightime only. In daytime, only elastic backscattered signals are measured. The laser beam can be linearly polarized and the elastic return is split by a polarizing cube that permits the separate recording of the polarization conserving backscattered signals and the cross polarized ones. The duration of a single acquisition is 70 s.

The PBL height can be derived from lidar measurements by different techniques. Among them the gradient of the range corrected signal and the measure of the fluctuations of the signal represent the commonly used techniques

(Flamant et al., 1997; Lammert and Bösenberg, 2006). In a recent paper the different techniques are reviewed and the results of continuous measurements are compared with the output of the mesoscale model COSMO (Baars et al., 2008). Both these methods rely on the fact that most of the pollutants, like aerosols, are concentrated in the PBL. Thus, at the boundary between the mixing layer and the free troposphere (or the residual layer) a large decrease in concentration of aerosols is observed as a steep decrease of the range corrected signal. If we define the lidar signal as $S(z)$, we can calculate the quantity:

$$D(z) = \frac{d}{dz}\left(\ln \frac{S(z)}{S_{mol}(z)}\right) \tag{1}$$

where $S_{mol}(z)$ is the calculated signal due to molecular backscattering only. The relative minima of this quantity identify the transitions between different layers. Usually, the first minimum identifies the mixing layer height.

From another point of view, the turbulent nature of the mixing layer makes for a fluctuating boundary between the PBL and the free troposphere. Measurements of such fluctuations by the standard deviation of the lidar signals as a function of the altitude allows for the determination of the PBL height.

Let $S(t_i, z)$ be a series of consecutive lidar signals. At each altitude we can calculate the relative standard deviation over $N+1$ signals, where N is assumed to be an even number, by the following relationship:

$$F_{N+1}(t_i, z) = \frac{\sigma_{N+1}(S(t_i, z))}{< S(t_i, z) >_{N+1}} \tag{2}$$

where

$$\sigma_{N+1}(S(t_i, z)) = \frac{\sqrt{\sum_{j=i-N/2}^{i+N/2}(S(t_j, z) - < S(t_i, z) >_{N+1})^2}}{N+1} \tag{3}$$

is the standard deviation and

$$< S(t_i, z) >_{N+1} = \frac{\sum_{j=i-N/2}^{i+N/2} S(t_j, z)}{(N+1)} \tag{4}$$

the average of the $N+1$ signals. The maximum of $F_{N+1}(t_i, z)$ identifies the PBL height. The number $N+1$ of profiles used for the calculation determines the temporal resolution of the measurement.

The two methods have advantages and drawbacks and should be used together because they are complementary to each other. The fluctuation method has the advantage that in principle it is independent of the lidar overlap function (Wandinger, 2005). Therefore, it can also be used at partial overlap altitudes. It is also independent of slowly changing properties of the lidar, like drifts in laser energy or misalignments, but it cannot be used in a stable PBL. We will report in the next section PBL height measurements based on the fluctuations method, but we have verified that the gradient method gives, in this case, similar results.

In this study, we have used also wind intensity and direction measured at an height of 20 m above ground by a standard meteorological station (Laboratorio di Micrometeorologia, Universitá del Salento, http://labmicrometeo.unisalento.it/index.htm) and data from a micrometeorological station to measure turbulent fluxes (CNR-ISAC, http://www.basesperimentale.le.isac.cnr.it/). Both stations are located at a distance less than 1 km far from the lidar site. The micrometeorological station is located at 16 m height over a grass soil. The data used and the corresponding instruments are :

- 3D 20 Hz wind speed vector and air temperature from a sonic anemometer SOLENT- Gill Research ,
- water vapour concentration from an hygrometer Campbell kH2O,
- surface temperature from a thermoradiometer Everest 4000.4GL,
- net radiation from a MICROS RADNT radiometer

The buoyancy and momentum fluxes (Q_s and τ_s), and the turbulent kinetic energy (TKE) are obtained from air temperature, vertical (w) and horizontal (u, v) wind components, water vapour mass mixing ratio (r), following the formulae in (Stull, 1988), where the averages are made over 30 minutes and the primed quantities represent fluctuations from the average:

$$Q_s = < \theta_v' w' >, \tag{5}$$

$$\tau_s = (< u'w' >^2 + < v'w' >^2)^{1/2}, \tag{6}$$

$$TKE = \frac{1}{2}(< u'^2 > + < v'^2 > + < w'^2 >), \tag{7}$$

and $\theta_v = \theta(1 + 0.61\, r)$ is the virtual potential temperature.

Finally, the meteorological station of Brindisi, which is located on the Adriatic Sea, about 40 km north-west of the lidar site (40.65 N,17.95 E), provides systematic radiosounding at least every 12 hours (http://www.esrl.noaa.gov/). The next closest radiosounding station is several hundred kilometres away.

4 Measurements

In the following, the time coordinate used is UTC+1 hour, which is about 7 minutes to the local solar time (LST); for simplicity, we will neglect this difference and we will refer our time coordinate as LST. Lidar measurements have been performed on July 14 from 0100 until 1510 LST , with some small gaps. We will focus here on measurements performed during daytime, starting at 0440 LST. Sunrise time is 0429 LST.

The synoptic map shows that an anticyclonic area centred on the British isles affected western Europe both at low and upper levels, as it can be seen from Fig. 2a. Only few clouds in the surroundings of the lidar site were present as can be seen from the net radiation plot of Fig. 2b (dotted line). The difference between the surface temperature and the air temperature at 16 m (Fig. 2b, solid line), which is representative of the convective forcing (Stull, 1988),

increases after sunrise until 1230 LST, then it decreases regularly until sunset. This difference becomes positive about one hour after sunrise, indicating that an effective heating of the ground takes place. At this point we expect that the PBL height grows rapidly, after the destabilization of the nocturnal stable layer, and that it reaches an almost constant height that is maintained until the afternoon (Stull, 1988).

Fig. 3a shows a colour map of the quantity $F_5(t_i, z)$ that has been obtained by applying the fluctuation method to the collected lidar signals. The highest fluctuation values, corresponding to the PBL height, are clearly revealed. As expected, the onset of the convection takes place about 1 hour after sunrise. Before this time, the analysis of the signal gradient shows that the PBL height is lower than 350 m, however its determination is uncertain because of the overlap function of the lidar.

We can notice from Fig. 3a that the PBL height increases until about 0900 LST; after a gap in measurements of about 40 minutes, during which it still increased, it stays constant at a value of about 900-1000 m until 1100 LST, then it abruptly decreases. After 1230 LST the PBL height is almost constant at 600-700 m. Between 1100 and 1400 LST, the PBL height is less well defined: there is not a sharp peak in the standard deviation space-time plot. However, $F_5(t_i, z)$ values abruptly decrease above a certain altitude, corresponding to the green-red transition in Fig. 3a. Therefore this altitude can be used to identify the PBL height. Our conclusion is supported by the gradient method results. To summarize, we can say that in this case the PBL height reaches a relative minimum around local noon, while we expect, on the contrary, as discussed in the introduction and as a consequence of the air-surface temperature difference, that it should be maximum.

The analysis of ground meteorological observations helps understanding the above reported evolution of the PBL height. First of all, measurements of the wind speed and direction at an altitude of about 20 m from the ground show that the wind direction (Fig. 3a, dotted line) veers during the day from west-north-west in the early morning to north-north-east in the warmest hours. This seems to be a typical sea breeze effect that makes the wind direction closer to that perpendicular to the coastline. An abrupt change of the wind direction, from north-west to north-north-east, is observed at 1010 LST about one hour before observing the PBL height decrease revealed in Fig. 3a. We can also observe from Fig. 3a (full line) that the wind speed increases at 1030 LST. Thus, referring to Fig. 1, it can be argued that, in the first part of the morning, air parcels arrive at the lidar site after travelling along the peninsula axis; after the veering of the wind, air parcels are advected directly from the sea, and the time they spend over land is much smaller. In the next sections we will provide a deeper insight to this observation.

The temporal evolution of the air temperature at 16 m (Fig. 3b, squares) and the water vapour concentration (Fig. 3b, triangles) indicate that colder and more humid air has been advected directly from the sea after 1000 LST. As a consequence, the PBL measured characteristics are determined by the development of an internal boundary-layer.

Measurements of the kinematic heat flux (Fig. 3c, squares) and momentum flux (Fig. 3c, circles) show a steep absolute value increase after the wind veering. This indicates an increase of the turbulence, which is confirmed by the fact that the lidar standard deviation (Fig. 3a, colour plot) displays a broader maximum after 1100 LST, and by the increase of the measured turbulent kinetic energy (Fig. 3d, circles). It is expected that strong turbulence is present in the internal boundary-layer, as a consequence of the advection of colder air on a warm soil (Gryning and Batchvarova, 1990).

Finally, there is another physical quantity that can further confirm that air properties have actually changed after the veering of the wind. We mention that the depolarization of the backscattered light depends on the shape of the aerosol particles (Sassen, 2005). We expect that this property is constant in a mixed layer, unless we are dealing with hygroscopic particles in conditions of high relative humidity. Figure 4 shows the colour map of the volume depolarization ratio, which is the ratio between the cross polarized and polarization conserving signal, versus time and altitude. The absolute value of the depolarization has been obtained by imposing that, in absence of aerosol, it has the constant value of 0.014 corresponding to the molecular depolarization. The value of the PBL height from Fig. 3a, averaged over 1 hour, is evidenced by open circles. As expected, we can see that the depolarization ratio is almost uniform inside the boundary-layer, apart from a first layer of about 100 m. After the wind veering, it significantly increases. This is a signature that aerosol types within the PBL have changed. This last result is consistent with the studies of Murayama et al. (1999) on the depolarization of aerosol observed in a sea breeze regime. Marine aerosol containing a higher content of NaCl crystals can actually produce larger depolarization ratios.

Such an effect could in principle be detected by sun photometer measurements. In fact, a photometer of the AERONET network is co-located with the lidar system. The data for this day are available on the web site of the network, and the value of the 450-870 nm Angstrom coefficient is plotted in Fig. 4. It is expected that the increase of depolarization should be associated to a decrease of the Angstrom coefficient, because the contribution of NaCl particles should contribute to an increase of the average dimension of aerosols. The 440-870 nm Angstrom coefficient actually decreases in the morning from 2 to 1.8, and its minimum is obtained at 1100 LST, after which its value increases back to 2. This minimum is correlated with the maximum in depolarization ratio observed around the wind veering, observed mainly at low altitudes.

Similar effects of lowering of the PBL height as a consequence of sea breezes or, in general, changing wind directions producing fetch variations, are reported in the literature, e.g Steyn and Oke (1982); Batchvarova and Gryning (1998); Batchvarova et al. (1999); Puygrenier et al. (2005). The peculiarity of this case is, on the one hand, the simplicity of the terrain that allows a direct interpretation, and, on the other hand, the fact that we can observe a transition between a continental boundary-layer and an internal boundary-layer triggered by the sea-breeze.

5 Comparison with the WRF model

5.1 Overview of PBL height evaluation in mesoscale models

Model parameterization schemes provide numerical values of the PBL height, but have to be considered as an over-simplification of the real world. Hanna et al. (1985) found that the root mean square error of the values from numerical models were often twice as large as the observed variability. The situation has certainly improved since then, as nonhydrostatic models with a few km resolution and more accurate turbulence closures are widespread research tools and in the last few years are becoming to be used as operational models. Nowadays, one-dimensional models with local turbulence closure of the order of 1.5, 2 or even higher have been used to estimate the height of the stable boundary-layer. Prognostic equations describing the growth of the convective boundary-layer are normally derived from the parameterization of the TKE budget equation. However, the variety of the methods and the rules which were applied to define the PBL height is quite large and the model results have been rarely compared with comprehensive observational datasets.

The PBL height extracted from the HIRLAM (http://hirlam.org/) output data has been defined as the height where the bulk Richardson number reaches a critical value, typically 0.25 (Gryning and Batchvarova, 2003). Berge and Jakobsen (1998) defined mixing heights from HIRLAM output differently, as the largest value between a mechanical mixing height and a convective mixing height.

Another method has been applied by Wotawa et al. (1996) to ECMWF model output. They determined a mechanical mixing height from the friction velocity, while a convective mixing height was determined from the temperature and the humidity profiles and the respective surface fluxes with the parcel method by Beljaars and Betts (1993). Under unstable conditions, the maximum of the two values was used.

Maryon and Best (1992) compared different methods for the calculation of PBL height. Most of these methods, based on the identification of the level where a critical gradient Richardson number (a value of 1.3 was chosen for the diagnosis from models) was reached, gave poor results. A simple parcel method, that determined the height as the lowest model level where the potential temperature exceeded the surface value, gave the best results.

Recently, the height of the planetary boundary-layer (PBL) has been diagnosed from COSMO model (http://www.cosmo-model.org/) outputs. Several methods have been tested for this purpose, using, e.g., the model bulk and gradient Richardson number, TKE or heat and momentum fluxes (in these cases, the PBL height is defined as the level where the turbulent kinetic energy or, respectively, the fluxes are reduced to a small percentage of the surface value). Methods based on the bulk Richardson number, TKE and momentum fluxes of the COSMO model have shown good agreements with measurements. However, in strongly convective situations the model tends to underestimate the PBL height (Szintai et al., 2009).

Two mesoscale models (MM5 and Meso-NH) simulated two clear-sky nights in the Iberian Peninsula using the same initial specification of input parameters, then the results were intercompared and checked with respect to field measurements (Bravo et al., 2008). Both models had difficulties in reproducing correctly the evolution of the wind direction and tended to overestimate the wind speed.

In conclusion, the mesoscale models are not yet able to simulate the structure of PBL in all its complexity, especially in situations with strong horizontal inhomogeneities. The accuracy of the calculated PBL height depends mainly on the degree of sophistication of the boundary-layer parameterization scheme and of the land-surface model.

5.2 Numerical simulations

Keeping in mind the limitations described in the previous sub-section, a state-of-the-art limited area model has been implemented over the Apulia region in order to simulate the evolution of PBL height and compare it with lidar observations. The Weather Research and Forecast (WRF) model, version ARW-3.0 (Michalakes et al., 2005; Klemp et al., 2007) has been developed in a cooperative effort coordinated by the National Center for Atmospheric Research, NCAR (USA); it is a numerical weather prediction system designed to serve both operational forecasting and atmospheric research needs. Two domains, with a two-way nesting configuration, have been implemented in the control experiment (hereafter CTL): the external domain (grid 1), with an horizontal resolution of 16 km, covers approximately the central Mediterranean basin, while the inner domain (grid 2), that has a resolution of 4 km, covers the southern Italy and adjacent seas. Forty vertical levels are employed, more closely spaced in the PBL (15 levels are present in the lowest 150 hPa). The simulations started at 0001 LST, 14 July 2006, and lasted for 24 hours. Initial and boundary conditions on the external grid were provided by the ECMWF analysis/forecasts.

In the simulations discussed here, the land-surface model (LSM) is the Noah LSM (Chen and Dudhia, 2001). This is a 4-layer soil temperature and moisture model with canopy moisture and snow cover prediction. It includes root zone, evapotranspiration, soil drainage, and runoff, taking into account vegetation categories, monthly vegetation fraction, and soil texture. The Mellor-Yamada-Janjic (MYJ) PBL scheme (Janjic, 1990, 1996, 2002) has been selected to parameterize the boundary-layer. MYJ represents an implementation of the Mellor-Yamada Level 2.5 turbulence closure model (Mellor and Yamada, 1982) through the full range of atmospheric turbulent regimes. In this implementation, an upper limit is imposed on the master length scale, that depends on TKE as well as the buoyancy and shear of the driving flow. The TKE production/dissipation differential equation is solved iteratively.

The evolution of the PBL height in the lidar site, as calculated in the CTL simulation, is shown in Fig. 5a. In agreement with the lidar measurements,

the model simulates a significant increase of the PBL height from 0700 LST (about 400 m) to 1000 LST (about 1000 m). After two hours during which the model simulates an almost constant PBL height, WRF predicts a decrease of the PBL height down to 800m, mainly concentrated between 1200 and 1400 LST. The model slightly delays and underestimates this decrease compared to the observations. Also, the model misses the PBL height increase observed after 1200 LST. Nevertheless, the model seems able to support the hypothesis that, while a continental boundary-layer develops inside Salento, a sea breeze develops in the morning close to the coastlines, so that the continental air mass is partly replaced by cooler maritime air next to the Adriatic and the Ionian seas. As a consequence, the PBL height still grows inside the peninsula from 1100 to 1300 LST, while an internal boundary-layer develops close to the coastline so that the retrieved PBL heights decrease as it is shown in the colour plot in Fig. 5b.

As suggested by an anonymous reviewer, the 4-km horizontal mesh size may be probably too coarse to reproduce the detailed IBL development and evolution. A posteriori, this idea is supported by a new simulation (hereafter HRES) with three different domains, where the two-way nesting acts both between the first and the second, and the second and the third grids. The run is performed using an additional domain (grid 3) with horizontal grid resolution of 1 km and centred over Salento peninsula. This simulation shows that the breeze front moves almost above the lidar site, with a PBL height horizontal gradient of few hundreds of metres in a few km (see Fig. 5c); as a consequence, a higher resolution experiment is really needed to better resolve such a strong horizontal inhomogeneity close to the instrument.

Fig. 5a shows that the new PBL height evolution simulated in the grid point corresponding to the lidar site in the second domain improves substantially the results obtained with the CTL run (as a two-way nesting technique is employed, the higher resolution grid is beneficial also for the coarser domain outputs). The evolution of the PBL height is phased with the observations, with a maximum at around 0900 LST and a decrease immediately afterward lasting a couple of hour, due to the penetration of marine air inland. Also, the PBL height increase observed in the lidar data immediately after 1200 LST is reproduced, although somehow overestimated by the model. However, such an improvement is not present in the grid point corresponding to the lidar site in the inner domain (where the PBL height evolution is similar to that simulated in the second grid of the CTL run, not shown), as the breeze front remains just to the east of the lidar site in the finer grid.

The fact that the decrease of the PBL height after 0900 LST is reproduced in HRES (grid 2) and not in CTL can be ascribed to a deeper penetration of the marine air inland in HRES with respect to CTL, probably due to an earlier triggering of the sea breeze. This hypothesis is supported by the different orientation of the wind vectors to the north/north-west of the lidar site a couple of hours earlier (not shown).

In conclusion, on the one hand, the use of a high resolution inner grid adds skill to the model results, at least in the sense described above. Previous

studies on sea breezes showed that finer horizontal resolution provides more accurate predictions (Case et al., 2002) through a better representation of the local terrain features. On the other hand, the point-by-point comparison with the lidar measurement of PBL height is worse in grid 3 than in grid 2. A limitation in the use of such high resolutions for sea breeze simulations was reported in Zhang et al. (2005) and Colby (2004). Both these studies noted that, although high resolution simulations show improvements with respect to coarser runs in reproducing observed sea breezes, statistical analysis at the observation stations may be locally even worse than in the coarser domains. Also, horizontal scales of O(1 km) are close to the "no man's land"separating classical PBL from large eddy simulation schemes (Weisman et al., 2005). As a result, the quality of the model physics (e.g., parameterization of the planetary boundary-layer and surface heat and moisture budget parameterizations) may be questionable, affecting the ability of mesoscale models to accurately reproduce atmospheric phenomena on such fine spatial scales with the current parameterization schemes at these resolution, particularly in terms of near-surface flow parameters.

Finally, we note that the assimilation of local data could provide a more accurate initial condition to initialize the model with and improve the model results. However, this approaches is left for a future study.

6 PBL height time evolution by a simple model

6.1 Description of the model

The results of the previous section show that a state of the art mesoscale model can reproduce fairly well the observed evolution of the PBL height, but cannot catch exactly the details of the process. As an alternative approach, it is interesting to use a simpler model that allows a more direct physical interpretation of the observed results and that can be fed with measured parameters.

Different authors (e.g. Steyn and Oke (1982)) have developed models to describe the evolution of the thermal internal boundary-layer at a coastal site, and Garratt (1990) provides a review. Most of these models originate from the Carson-Tennekes (Carson, 1973; Tennekes, 1973) formulation for the growth of PBL in neutral and unstable conditions over homogeneous terrain and share the feature that, in the equations used to describe the PBL evolution, time derivatives are replaced by total time derivatives.

In particular, we start here from the formulation of Gryning and Batchvarova (1996) in which the 2D variation of the PBL height is taken into account. Such a model requires the solution of a partial derivative differential equations, and it has been shown that it performs well compared to a full 3D mesoscale model (Batchvarova et al., 1999). Luhar (1998) has extended this model to the case of neutral flows. We neglect the subsidence effect because on this day the observations are made on the east side of the anticyclonic area, and the correction applied by Luhar (1998) to take into account a null value

of the lapse rate, because in this case the flow is stable as indicated by the WRF model simulations. The notations are those used in Luhar (1998). The equation reads:

$$\frac{\partial H}{\partial t} + \mathbf{v} \cdot \nabla H = -\frac{Q_i}{\Delta} \tag{8}$$

where $H \equiv H(x, y, t)$ is the height of the internal boundary-layer, $\mathbf{v}$ is the mean horizontal wind velocity field, Q_i the buoyancy flux at the inversion height and Δ is the inversion strength. The parametrisation of Q_i (Zilitinkevich, 1975) gives:

$$\frac{\partial H}{\partial t} + \mathbf{v} \cdot \nabla H = \frac{C_k w_m^3}{C_T w_m^2 + gh\Delta/T} \tag{9}$$

where $w_m^3 = w_*^3 + C_N^3 u_*^3$, C_k, C_N, C_T are empirical constants ($C_k = 0.18, C_N = 1.33, C_T = 0.8$ (Luhar, 1998), u_* is the friction velocity (square root of the module of the kinematic momentum flux),$w_\star = (gHQ_s/T)^{1/3}$, Q_s is the buoyancy flux at the surface, g is the gravity acceleration, T is the absolute temperature at the surface. Following the parametrisation of Gryning and Batchvarova (1990), Δ is defined by:

$$\Delta = \frac{\gamma H(C_k H - C_k C_N^3 kL)}{(1 + 2C_k)H - 2C_k C_N^3 kL} \tag{10}$$

where L is the Obhukov length $L = -u_*^3 T/(kgQ_s)$, k is the von Karman constant $k = 0.4$, and γ is the potential temperature lapse rate above the internal boundary-layer.

This 2D formulation reduces to the simpler 1D case when the wind field is homogeneous and its direction is constant. In this case, the equation can be solved along a direction parallel to the mean wind. Furthermore, in the case the wind speed U and the other parameters are constant, a steady-state solution in the variables $x' = x$, $t' = t - x/U$, where x is the coordinate along the wind direction, can be found (Steyn and Oke, 1982; Gryning and Batchvarova, 1990; Luhar, 1998).

We are interested here in the solution of Eq. 8 at just one point, where experimental data are available. Martano (2002) has proposed an algorithm for solving the 1D version of Eq. 8 at one point, using the steady-state solution of the equation, following Gryning and Batchvarova (1990) and Luhar (1998) to evaluate the spatial derivative at the point of interest, reducing the problem to be time dependent only. His approach has been validated by comparison with SODAR measurements performed at our site. However, this method does not reproduce the details of the reported lidar measurements, probably because the change in the wind vector is too fast for comparison with a stationary solution. Instead, we integrate Eq. 8 along the trajectory of the air parcel that, at a generic time t_1, arrives in the point of interest $\mathbf{X}$. We call these trajectories as $\mathbf{x}(t, t_1)$; if the wind field is known, they can be found as backtrajectories (Stohl, 1998). From a mathematical point of view, this is a particular case of the method of characteristics (Courant and Hilbert, 1962) for solving partial

differential equations. From the physical point of view, this means following the lagrangian point of view and solving Eq. 8 in a reference frame moving with the air parcels along a trajectory determined by the wind field. Eq. 8 has the general form:

$$\frac{\partial H}{\partial t} + \mathbf{v} \cdot \nabla h = f(\mathbf{W}(\mathbf{x}, t), H) \tag{11}$$

where W is the field of all the parameters of the equation. Applying the method to the specific case, Eq. 8 becomes:

$$\frac{dh}{dt} = f(\mathbf{W}(\mathbf{x}(t, t_1)), h) \tag{12}$$

where $h(t) = H(\mathbf{x}(t, t_1), t)$ is now a function of time only.

As we will explicitly show later on, the synoptic conditions make the backtrajectories quite simple. Since the wind is north-westerly in the morning and rotates to north-easterly, we have two well-defined situations: a) the backtrajectory stays on the land from sunrise or, b) the backtrajectory crosses the coast after sunrise. This situation allows the defining of initial conditions. In the first case the initial condition can be set to the boundary-layer height when the diurnal convection has started. In the second case, which corresponds to the developing of an internal boundary-layer, the initial condition will be set to the mixed layer height at the coast line. In the case of a stable flow, this height can be set near zero; following Gryning and Batchvarova (1996) we expect that the exact value of the internal boundary-layer at the coast line is not important because a shallow PBL increases rapidly in a convective regime. A sensitivity study confirms this assumption as will be shown in the next section.

To summarize, the calculation of the PBL height h at a certain time t_1, at coordinates $\mathbf{X}$, follows three steps, supposing that the wind field and the other parameters fields in Eq. 8 are known:

- a) determination of the backtrajectory $\mathbf{x}(t, t_1)$
- b) determination of the initial time t_0 for the integration of Eq. 12 and the initial condition $h_0 = H(t_0, \mathbf{x}(t_0, t_1))$
- c) integration of the Eq. 12 from t_0 to t_1.

These steps are repeated at each time t_1 of interest.

6.2 Results of the model

Up to now, no approximation has been made and the solution $h(t_0, t)$ for $t < t_1$ will be the same as the general solution of the partial derivative differential equation when restricted to the backtrajectory $\mathbf{x}(t, t_1)$. The practical use of this model rests instead on approximations about the equation parameters and initial conditions. The potential temperature lapse rate has been obtained by the radiosounding profile in Brindisi at 1200 UTC, and assumed to be constant during the day with $\gamma = 0.025\, K\, m^{-1}$. We consider the parameters measured

at the lidar site as representative of a homogeneous field, i.e. we suppose that the wind field, air temperature, heat and momentum fluxes are the same over the Salento peninsula. This is not too strong an approximation because of the flatness and the homogeneity of the terrain. Backtrajectories are calculated using this homogeneous wind field and the result is shown in Fig. 6a. The initial conditions for backtrajectories starting on the coast after sunrise should correspond to the initial height of the internal boundary-layer. This quantity is not known but its value is not supposed to be critical (Batchvarova and Gryning, 1991). For a stable flow, it should be some tens of metres. We will use a variable value centred around 150 m, as it will be explained in the following. For backtrajectories ending on land at sunrise, we use the value of the PBL height as determined by the lidar measurements at the time t_{conv}=0610, about 1 hour and half after the sunrise. At this time the measured kinematic heat flux has become positive. The PBL height at this time is 410 m and this value will be used as initial condition.

Figure 6a shows that the backtrajectories arriving at Lecce from 0700 to 0900 are over land at time $t_0 = t_{conv}$. Trajectories from 1000 to 1400, instead, cross the coastline at a time $t^\star > t_{conv}$. Figure 6b shows the corresponding integration time, which is the time elapsed from t_{conv} for trajectories entirely over land, or the time elapsed from $t^\star$, the crossing time of the coast line, until the time t_1. The comparison of Fig. 6b with Fig. 3c reveals that, between sunrise and 0900 LST, the modulus of heat and momentum fluxes, that force the growth of PBL, increases and the interaction time also increases. In this case we can expect that the PBL height will also increase. After 0930 air parcels travel from the coast to the observation site, so that the height of the inversion is actually determined by the development of the internal boundary-layer. Between 0900 and 1030 the interaction time, determined by the fetch and the wind speed, is constant, the fluxes have a small variation, so that only small variations of the PBL height are expected. Between 1030 and 1130 LST, instead, the interaction time decreases rapidly so that we expect to observe a less developed internal boundary-layer; this is measured as a rapid decreasing of the PBL height. After this time, the interaction time is almost constant and we will expect an almost constant measured PBL height, corresponding to a quasi-stationary thermal internal boundary-layer with a constant fetch.

In Fig. 7, the comparison of the results of the integration of Eq. 12 with the measured PBL height shows a reasonably good agreement. The first part of the PBL growth, corresponding to trajectories entirely over land after t_{conv}, is equivalent to what can be obtained by just integrating the PBL model in a homogeneous terrain with the initial conditions specified above. This calculation, plotted as a solid line in Fig. 7 follows closely the measured PBL height until 0850, when the first series of lidar measurements has been stopped, and it is still in agreement with the measurement at 0945, when lidar measurements have been restarted. However, after this time, we can see that this calculation does not reproduce the measured PBL height as it is determined now by the development of the internal boundary-layer. The results of this calculation are represented as open squares in Fig. 7. The error bars represent the standard

deviation of the results obtained by randomly varying the initial condition from 10 m to 300 m and the interaction time by 25%.

The discrepancies between the measurements and the results of the model can be ascribed to the inadequacy of the hypothesis of uniform parameters and wind that will not be exactly followed, especially between 1000 LST and 1100 LST when the triggering of the sea breeze determines a transient situation. In particular, the value for the PBL height at 0940 LST (first open square) is underestimated, while the value obtained by the continental boundary-layer is in better agreement with the measurements. In this case, we are at the border between the two PBL growth regimes and a small uncertainty on the backtrajectory can determine a wrong choice between the two regimes.

However, the model reproduces the main results of the lidar measurements: the PBL height increases in the morning when the wind direction is almost parallel to the peninsula axis. In this case the development of PBL is equivalent to a continental PBL in a homogenous terrain. Later in the day, the wind turns eastward, which is expected because of the sea breeze, and in this case an internal boundary-layer develops from the coast; this is measured at the lidar site as a suppression of the PBL height growth and later as a decrease in the measured PBL height.

We can expect that this situation is quite general: in anticyclonic conditions, sea breeze usually develops when sun irradiation is maximum, i.e. around noon, thus it may be expected that PBL height is not maximum at this time. This phenomenon is less pronounced in winter time, so we can also expect that, on average, the PBL height measured around 1300 UTC be lower in summer than in winter. This last comment also allows us to understand the experimental results obtained during EARLINET measurements reported in De Tomasi and Perrone (2006), since EARLINET diurnal measurements are scheduled for 1300 UTC.

7 Conclusions

The PBL height has been measured by a lidar system in a peninsular site during a summer day in anticyclonic conditions (no clouds), starting from 0440 LST (11 minutes after sunrise) until the mid-afternoon. The closeness of the lidar site to the sea, about 15 km, makes the boundary-layer height very dependent on the history of air parcels. Depending on the wind direction, in fact, we can have a continental boundary-layer or an internal boundary-layer that grows spatially until an height depending mostly on the transit time of the marine air parcels to the measurements site. The analysis of the PBL heights retrieved during the measurements day reveals that at the beginning of the day the PBL height increases until 1000 LST, then it maintains constant at about 1000 m, and finally we observe at 1100 LST a sudden decrease of the PBL height associated with a wind veering, an increase of the turbulence, and a reduction of the air temperature. After this transition we observe a slow increase in the afternoon up to about 600-700 m. We interpret this behaviour

as a consequence of three different regimes of PBL growth: at the beginning of the day, a layer of about 350 m is present. The measured PBL height is the evolution of a PBL starting from the onset of convection, about 1 hour after sunrise. Then, air parcels come from the sea, originating an internal boundary-layer, and can interact with the warmed soil for a time of 2-3 hours, as it can be inferred from wind direction and intensity. This regime corresponds to the central part of the measurement hours in which the PBL height is maximum and can be reproduced by estimating the interaction time of marine air masses with the soil. Finally, the wind veering leads to an interaction time with the land of just about one hour, so that the measured PBL height is reduced to only 400 m, and stabilises after 1200 LST to 600-700 m.

This interpretation has been checked using the WRF model with ECMWF analysis data as initial/boundary conditions. Model runs suggest that the interpretation is realistic and the simulated boundary-layer height confirms the observed trend. To further confirm this interpretation, and looking for a simple model in which the interpretation of the results is more direct, we have also solved the Gryning-Batchvarova 2D model for the internal boundary-layer growth integrating along the trajectories arriving at the lidar site (characteristics method). The agreement is satisfactory, even though several assumptions for the parameter fields have been made.

In conclusion, this work shows that the PBL height at a coastal site can be highly variable and that its evolution can be counter-intuitive. Using temporal high resolution measurements, knowledge of the meteorological situation and a simple model, we could reproduce reasonably well the behaviour of the PBL height, which is a relevant result considering the importance of the PBL height for the determination of the concentration of pollutants and other applications. Finally, we expect that the results of this paper can be meaningful also for other coastal regions with a similar morphology.

8 Acknowledgements

This work has been partially funded by the EARLINET-ASOS project (European Commission, grant RICA-025991)and by the SIMPA project of Regione Puglia, Italy. Meteorological data have been provided by “Laboratorio di Micrometeorologia ”of Universitá del Salento. We thank Paolo Martano for discussions and providing experimental data from the micrometeorological station of CNR-ISAC, section of Lecce. Richard Rotunno, Umberto Giostra and Silvana Di Sabatino are gratefully acknowledged for the critical reading of the manuscript.

References

Abbs DJ, Physick WL (1992) Sea-breeze observations and modelling: a review. Aust Met Mag 41:7–19

Baars H, Ansmann A, Engelmann R, Althausen D (2008) Continuous monitoring of the boundary-layer top with lidar. Atmos Chem Phys 8:7281–7296

Batchvarova E, Gryning SE (1991) Applied model for the growth of the daytime mixed layer. Boundary-Layer Meteorol 56:261–274

Batchvarova E, Gryning SE (1998) Wind climatology, atmospheric turbulence and internal boundary-layer development in Athens during the MEDCAPHOT-TRACE experiment. Atmos Environ 32:2055 – 2069

Batchvarova E, Cai X, Gryning SE, Steyn D (1999) Modelling internal boundary layer development in a region with a complex coastline. Boundary-Layer Meteorol 90:1–20

Beljaars ACM, Betts AK (1993) Validation of the boundary layer representation in the ECMWF model. In: Validation of the models over Europe, ECMWF Seminar Proceedings, vol 2, pp 159–195

Berge E, Jakobsen HA (1998) A regional scale multi-layer model for the calculation of long-term transport and deposition of air pollution in Europe. Tellus 50:205–223

Boselli A, Armenante M, D'Avino L, D'Isidoro M, Pisani G, Spinelli N, Wang X (2009) Atmospheric aerosol characterization over Naples during 2000 - 2003 EARLINET project: Planetary boundary-layer evolution and layering. Boundary-Layer Meteorol 132:151–165

Bösenberg J, Matthias V, Amodeo A, Amoiridis V, Ansmann A, Baldasano J, Balin I, Balis D, Boeckmann C, Boselli A, Carlsonn A, Chaikowsky A, Chourdakis G, Comeron A, De Tomasi F, Eixmann R, Freudenthaler V, Giegl H, Grigorov I, Hagard A, Iarlori M, Kirsche M, Kolarov M, Komguen L, Kreipl M, Kumpf M, Larcheveque M, Linne H, Matthey R, Mattis I, Mekler A, Mironova I, Mitev V, Mona L, Muller D, Music S, Nickovic S, Pandolfi M, Papayannis A, Pappalardo G, Pelon J, Perez C, Perrone M, Persson R, Resendes D, Rizi V, Rocadenbosch F, Rodrigues J, Sauvage L, Scheidenbach L, Schumaker R, Shcherbakov V, Simeonov V, Sobolewski P, Spinelli N, Stachlewska I, Stoyanov D, Trickl T, Tsaknakis G, Vaughan G, Wandinger U, Wang X, Wiegner M, Zavrtanik M, Zerefos C (2003) A European aerosol research lidar network to establish an aerosol climatology. Tech. Rep. 348, Max-Planck- Institut fur Meteorologie, 191 pp

Bravo M, Mira T, Soler MR, Cuxart J (2008) Intercomparison and evaluation of MM5 and Meso-NH mesoscale models in the stable boundary layer. Boundary-Layer Meteorol 128:77–101

Carson DJ (1973) The development of a dry inversion-capped convectively unstable boundary layer. Q J Roy Meteorol Soc 99:450–467

Case JL, Manobianco J, Dianic AV, Wheeler MM, Harms DE, Parks CR (2002) Verification of high-resolution rams forecasts over east-central florida during the 1999 and 2000 summer months. Wea Forecasting 17:1133–1151

Chen F, Dudhia J (2001) Coupling an advanced land-surface/ hydrology model with the Penn State/ NCAR MM5 modeling system. part I: Model description and implementation. Mon Weather Rev 129:569–585

Colby FPJr (2004) Simulations of the New England sea breeze: The effect of grid spacing. Wea Forecasting 19:277–285

Courant R, Hilbert D (1962) Methods of Mathematical Physics, vol II. Interscience Publisher, 830 pp

Dayan U, Heffter J, Miller J (1996) Seasonal distribution of the boundary layer depths over the mediterranean basin. In: Guerzoni S, Chester R (eds) The Impact of Desert Dust Across the Mediterranean, Kluwer, pp 103–112

De Tomasi F, Perrone MR (2003) Lidar measurement of tropospheric water vapor and aerosols profiles over southern italy. J Geophys Res 108:10.1029/2002JD002,781

De Tomasi F, Perrone MR (2006) PBL and dust layer seasonal evolution by lidar and radiosounding measurements over a peninsular site. Atmos Res 80:86–103

Delbarre H, Augustin P, Saïd F, Campistron B, Benech B, Lohou F, Puygrenier V, Moppert C, Cousin F, Freville P, Frejafon E (2005) Ground-based remote sensing observation of the complex behaviour of the Marseille boundary layer during ESCOMPTE. Atmos Res 74:403 – 433

Flamant C, Pelon J, Flamant P, Durand P (1997) Lidar determination of the entrainment zone thickness at the top of the entrainment zone thickness at the top of the unstable marine atmospheric boundary layer. Boundary-Layer Meteorol 83:247–284

Garratt JR (1990) The internal boundary layer: a review. Boundary-Layer Meteorol 50:171–203

Garratt JR (1992) The atmospheric boundary layer. Cambridge University Press, Cambridge, 316 pp

Gryning SE, Batchvarova E (1990) Analytical model for the growth of the coastal internal boundary layer during onshore flows. Q J Roy Meteorol Soc 116:187–203

Gryning SE, Batchvarova E (1996) A model for the height of the internal boundary layer over an area with irregular coastline. Boundary-Layer Meteorol 78:405–413

Gryning SE, Batchvarova E (2003) Marine atmospheric boundary-layer height estimated from nwp model output. Int J Environ Pollut 20:147–153

Haeffelin M, Morille Y, Görsdorf U, Teschke G, Beyrich F (2009) Retrieval of mixing layer depth from existing ceilometer/lidar networks in Europe. In: 8th International Symposium on Tropospheric Profiling: Integration of Needs, Technologies and Applications. 19-23 October 2009, Delft, The Netherlands, paper S10-002

Hanna SR, Burkhart CL, Paine RJ (1985) Mixing height uncertainties. In: Proceedings of 7th AMS Symposium on Turbulence and Diffusion, pp 82–85

Janjic ZI (1990) The step-mountain coordinate: physical package. Mon Weather Rev 118:1429–1443

Janjic ZI (1996) The surface layer in the NCEP Eta Model. In: 11th Conference on Numerical Weather Prediction, 19-23 August, Norfolk,VA, pp 354–355

Janjic ZI (2002) Nonsingular implementation of the Mellor-Yamada level 2.5 scheme in the NCEP Meso model. Tech. rep., NCEP, 437, 61 pp

Klemp JB, Skamarock WC, Dudhia J (2007) Conservative split-explicit time integration methods for the compressible nonhydrostatic equations. Mon Weather Rev 135:2897–2913

Lammert A, Bösenberg J (2006) Determination of the convective boundary-layer height with laser remote sensing. Boundary-Layer Meteorol 119:159–170

Lemonsu A, Bastin S, Masson V, Drobinski P (2006) Vertical structure of the urban boundary layer over Marseille under sea-breeze conditions. Boundary-Layer Meteorol 118:477–501

Luhar A (1998) An analytical slab model for the growth of the coastal thermal internal boundary layer under near neutral on shore flow conditions. Boundary-Layer Meteorol 89:385–405

Luhar AK, Sawford BL, Hacker JM, Rayner KN (1998) The Kwinana Coastal Fumigation Study: II growth of the thermal internal boundary layer. Boundary-Layer Meteorol 88:103–120

Mangia C, Martano P, Miglietta MM, Morabito A, Tanzarella A (2004) Modeling local winds over the Salento peninsula. Meteorol Appl 11:231–244

Martano P (2002) An algorithm for the calculation of the time dependent mixing height in coastal site. Jour Appl Meteorol 41:351–354

Maryon RH, Best MJ (1992) 'NAME', 'ATMES' and the boundary layer problem. Turbulence and Diffusion Note. Tech. Rep. 204, UK Meteorological Office

Mastrantonio G, Viola AP, Argentini S, Fiocco G, Giannini L, Rossini L, Abbate G, Ocone R, Casonato M (1994) Observations of sea breeze events in Rome and the surrounding area by a network of Doppler sodars. Boundary-Layer Meteorol 71:67–80

Matthias V, Balis D, Bösenberg J, Eixmann R, Iarlori M, Komguem L, Mattis I, Papayannis A, Pappalardo G, Perrone MR, Wang X (2004) Vertical aerosol distribution over europe: Statistical analysis of raman lidar data from 10 european aerosol research lidar network (EARLINET) stations. J Geophys Res 109:D18,201

McCormick P (2005) Airborne and spaceborne lidar. In: Weitkamp CE (ed) Lidar:Range-Resolved Optical Remote Sensing of the Atmosphere, Springer Series in Optical Sciences , Vol. 102, chap 13, pp 355–397

McElroy JL, , Smith TB (1991) Lidar descriptions of mixing-layer thickness characteristics in a complex terrain/coastal environment. J Appl Meteor 30:585597

McQueen JT, Tassone C, Tsidulko M, Zhu Y, Cucurull L, Liu S, Manikin G, DiMego G (2010) An overview of the NOAA/NWS/NCEP real-time mesoscale analysis (RTMA) system with extensions for the atmospheric boundary layer. In: 16th Conference on Air Pollution Meteorology, 17-21 January 2010, Atlanta, GA, paper 7.6

Melas D, Kambezidis HD (1992) The depth of the Internal Boundary Layer over an urban area under sea-breeze condition. Boundary-Layer Meteorol 61:247–264

Melas D, Ziomas I, Zerefos C (1995) Boundary layer dynamics in an urban coastal environment under sea-breeze conditions. Atmos Environ 29:3605–3617

Mellor GL, Yamada T (1982) Development of a turbulence closure model for geophysical fluid problems. Rev Geophys Space Phys 20:851–875

Michalakes J, Dudhia J, Gill D, Henderson T, Klemp J, Skamarock W, Wang W (2005) The Weather Research and Forecast model: Software architecture and performance. In: Zwieflhofer W, Mozdzynski G (eds) 11th ECMWF Workshop on the Use of High Performance Computing in Meteorology, World Scientific, pp 156–168

Miller STK, D KB, Talbot RW, Mao H (2003) Sea breeze: Structure, forecasting, and impacts. Reviews of Geophysics 41(3):1011

Murayama T, Okamoto H, Kaneyasu N, Kamataki H, Miura K (1999) Application of lidar depolarization measurement in the atmospheric boundary layer: effects of dust and sea-salt particles. J Geophys Res 104:31,78131,792

Puygrenier V, Lohou F, Campistron F, Said F, Pigeon G, Benech B, Serça D (2005) Investigation on the fine structure of sea-breeze during ESCOMPTE experiment. Atmos Res 74:329–353

Santacesaria V, Marenco F, Balis D, Papayannis A, Zerefos C (1998) Lidar observations of the planetary boundary layer above the city of Thessaloniki, Greece. Nuovo Cimento C 21(6):585–595

Sassen K (2005) Polarization in lidar. In: Weitkamp CE (ed) Lidar:Range-Resolved Optical Remote Sensing of the Atmosphere, Springer Series in Optical Sciences , Vol. 102, chap 2, pp 19–42

Seibert P, Beyrich F, Gryining SE, Joggre S, Rasmussen A, Tercier P (2000) Review and intercomparison of operational methods for the determination of the mixing height. Atmos Environ 34:1001–1027

Sicard M, Perez C, Rocadenbosch F, Baldasano JM, Garcia-Vizcaino D (2006) Mixed-layer depth determination in the Barcelona coastal area from regular lidar measurements: Methods, results and limitations. Boundary-Layer Meteorol 119:135–157

Simpson JE (1994) Sea breeze and local winds. Cambridge University Press, Cambridge, 234 pp

Steyn DG, Oke TR (1982) The depth of the daytime mixed layer at two coastal sites: a model and its validation. Boundary-Layer Meteorol 24:161–180

Steyn DG, Bottenheim JW, Thomson RB (1997) Overview of tropospheric ozone in the Lower Fraser Valley, and the Pacific '93 field study. Atmos Environ 31(14):2025–2035

Stohl A (1998) Computation, accuracy and applications of trajectories: a review and bibliography. Atmos Environ 32:947–966

Stull RB (1988) Introduction to boundary layer meteorology. Kluwer Academic Publisher, 670 pp

Szintai B, Kaufmann P, Rotach MW (2009) Deriving turbulence characteristics from the COSMO numerical weather prediction model for dispersion applications. Adv Sci Res 3:79–84

Talbot C, Augustin P, Leroy C, Willart V, Delbarre H, Khomenco G (2007) Impact of a sea breeze on the boundary-layer dynamics and the atmospheric stratification in a coastal area of the North Sea. Boundary-Layer Meteorol 125:133–154

Tennekes H (1973) A model for the dynamics of the inversion above a convective boundary layer. J Atmos Sci 30:558–567

Wandinger U (2005) Introduction to lidar. In: Weitkamp CE (ed) Lidar:Range-Resolved Optical Remote Sensing of the Atmosphere, Springer Series in Optical Sciences , Vol. 102, chap 1, pp 1–18

Wauben WMF, de Haij M, Baltink HK (2008) Towards a cloud ceilometer network reporting mixing layer height. In: TECO-2008 - WMO Technical Conference on Meteorological and Environmental Instruments and Methods of Observation-St. Petersburg,Russian Federation, 27-29 November 2008, paper P1(5)

Weisman M, Davis C, Wang W (2005) Explicit convective forecasting with the wrf model. In: WRF-MM5 Workshop, June 30, Boulder, CO

Wotawa G, Stohl A, Kromb-Kohl H (1996) Parameterization of the planetary boundary layer over Europe: a data comparison between the observation-based OML preprocessor and ECMWF model data. Contr Atmos Phys 69:273–284

Zhang Y, Chen YL, Schroeder TA, Kodama K (2005) Numerical simulations of sea-breeze circulations over northwest Hawaii. Wea Forecasting 20:827–846

Zilitinkevich S (1975) Comments on: A model for the dynamics of the inversion above a convective boundary layer. J Atmos Sci 32:991–992

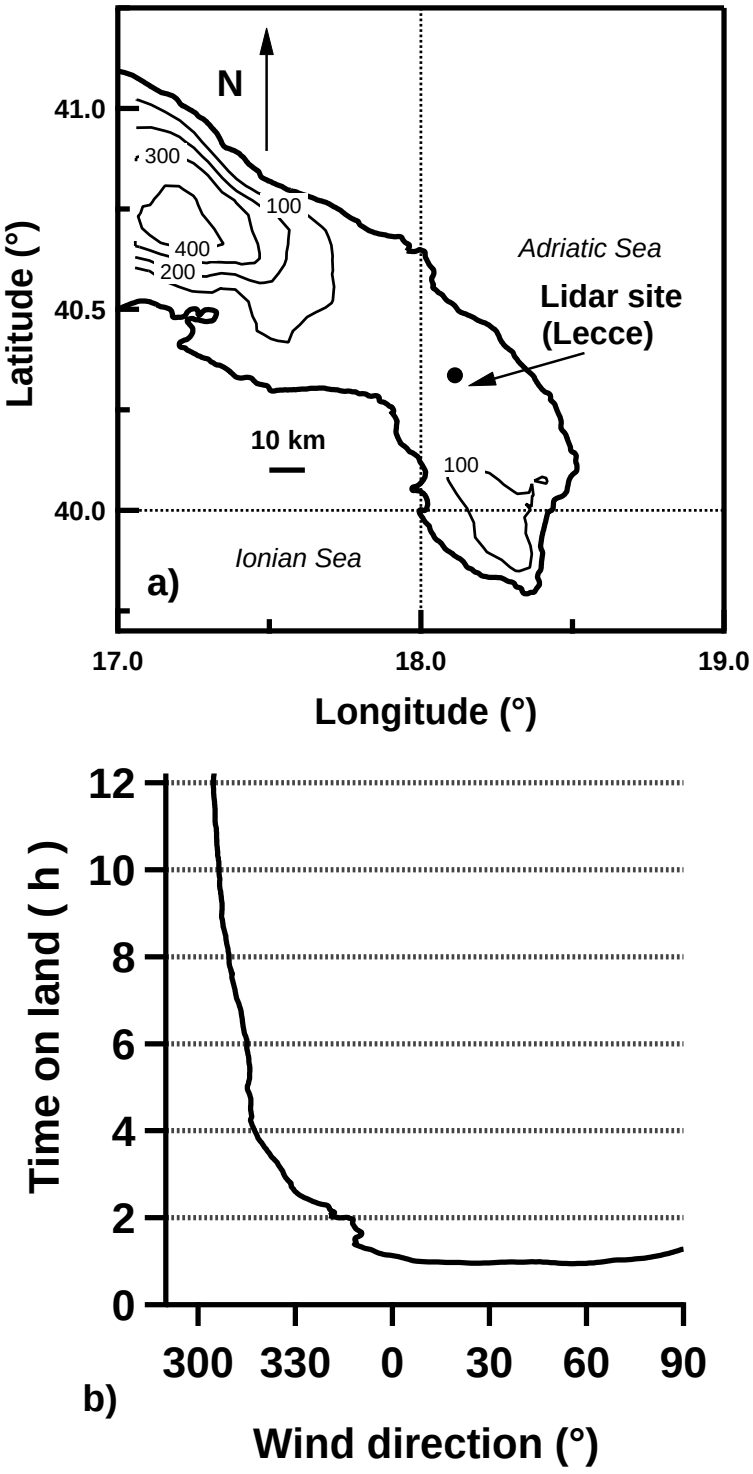

Fig. 1 a) Map of the Salento peninsula and location of the lidar site. b) Time spent on the land by an hypotethical air parcel travelling with a speed of (5 m s^{-1}) from the coast to the lidar site along a straight line as a function of the wind direction.

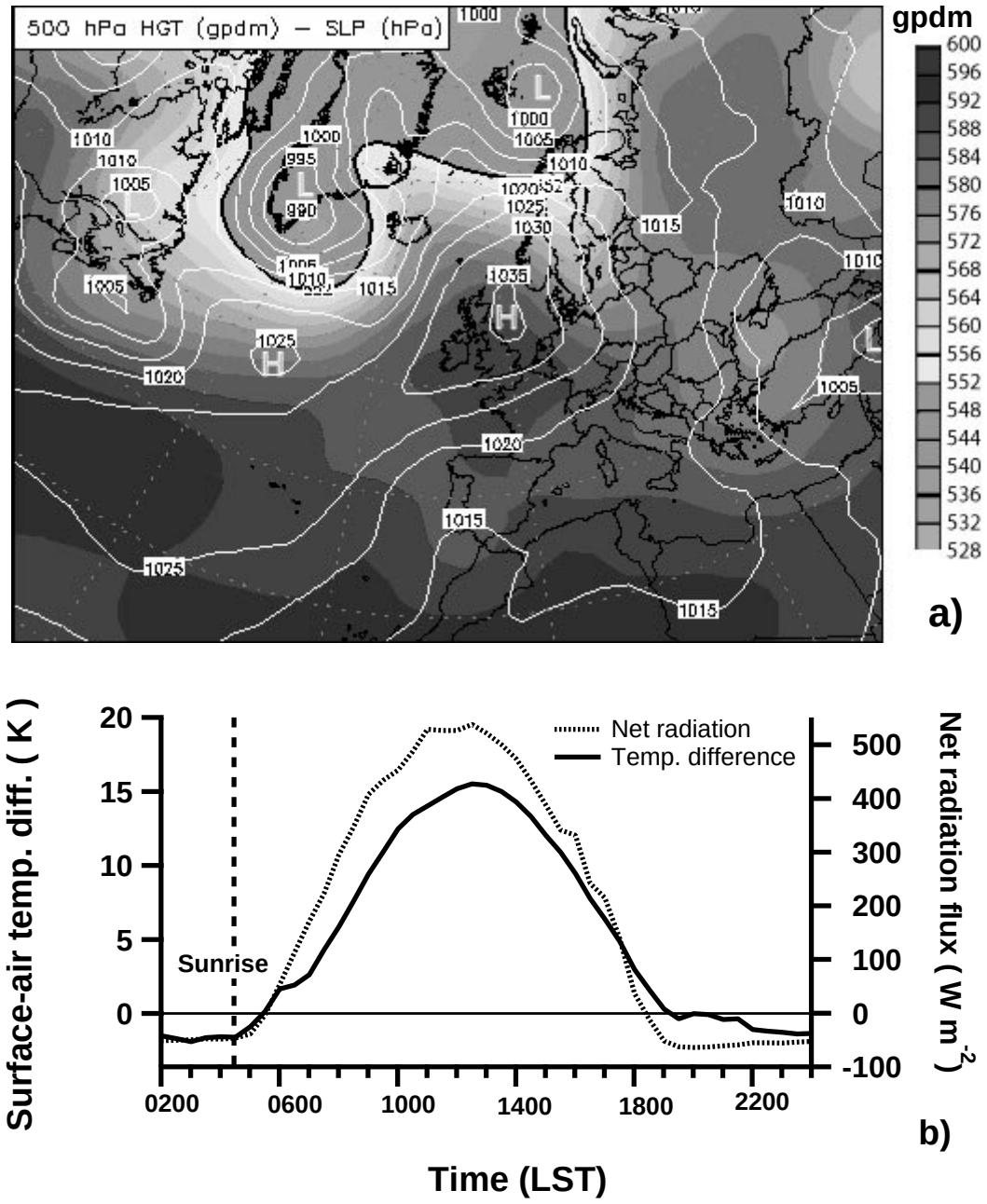

Fig. 2 a) Synoptic chart for Europe on July 14, 2006, showing the sea level pressure (hPa, level curves) and the 500 hPa geopotential height (geopotential decametre, grey tones). b) Net radiation (dashed line) and difference between surface and 16 m air temperature (solid line) measured at the lidar site.

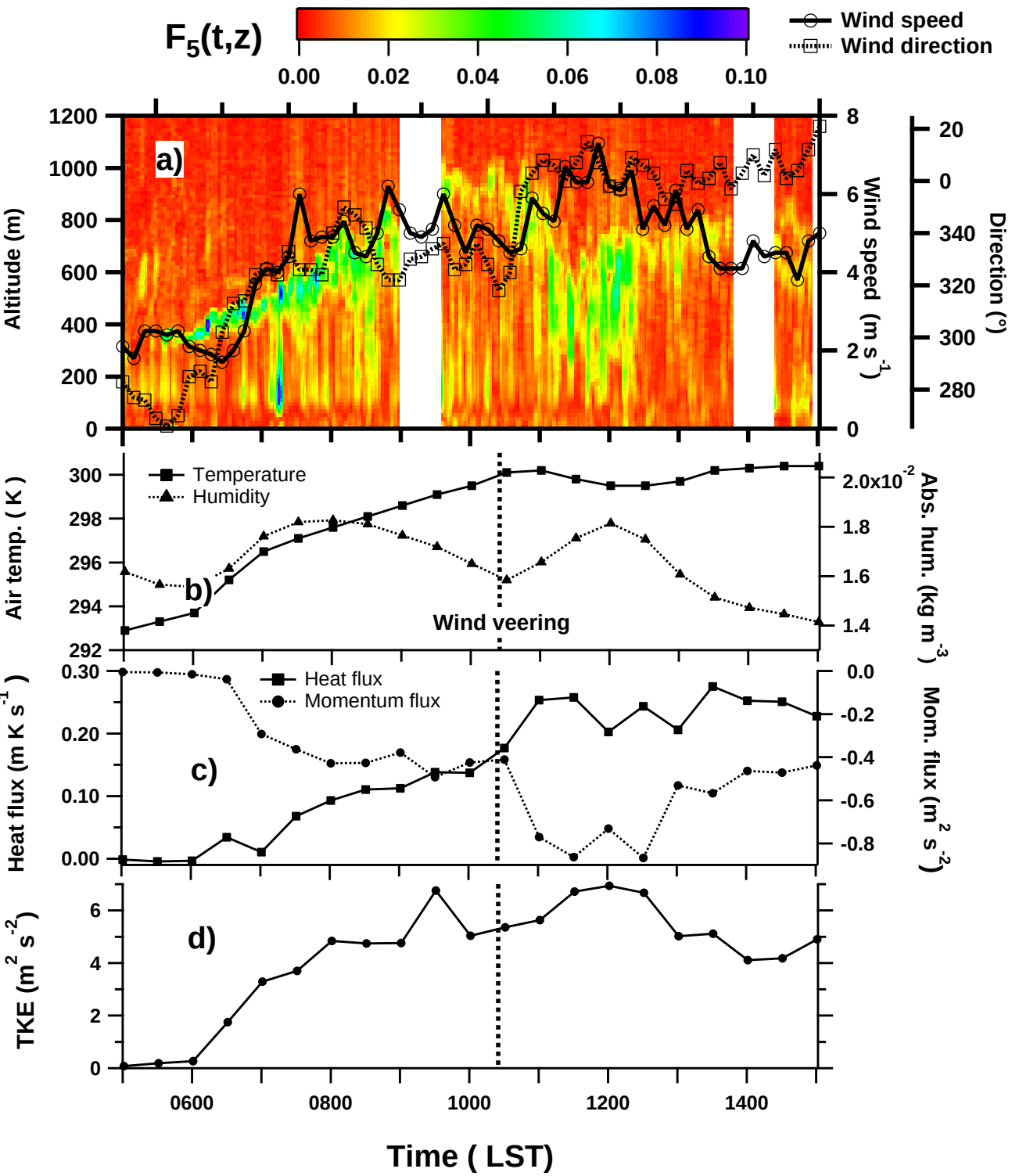

Fig. 3 a) Colour map of the relative standard deviation $F_5(z,t)$ which has been calculated over 5 consecutive lidar profiles, corresponding to a total time of six minutes. Wind intensity (solid line) and direction (dotted line) are superimposed. b)-d) Data from the micrometeorological station at 16 m. b)Air temperature (squares) and water vapour concentration (triangles). c) Kinematic heat flux (squares) and momentum flux (circles) flux. d) Turbulent kinetic energy.

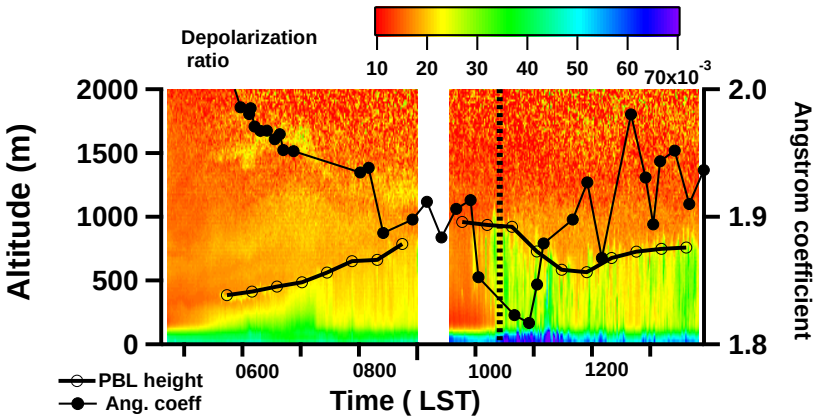

Fig. 4 Colour map of the volume depolarization ratio. Round open circles represent the PBL height averaged over 30 minutes. Full circles are the Angström coefficient as measured by a co-located AERONET sun photometer.

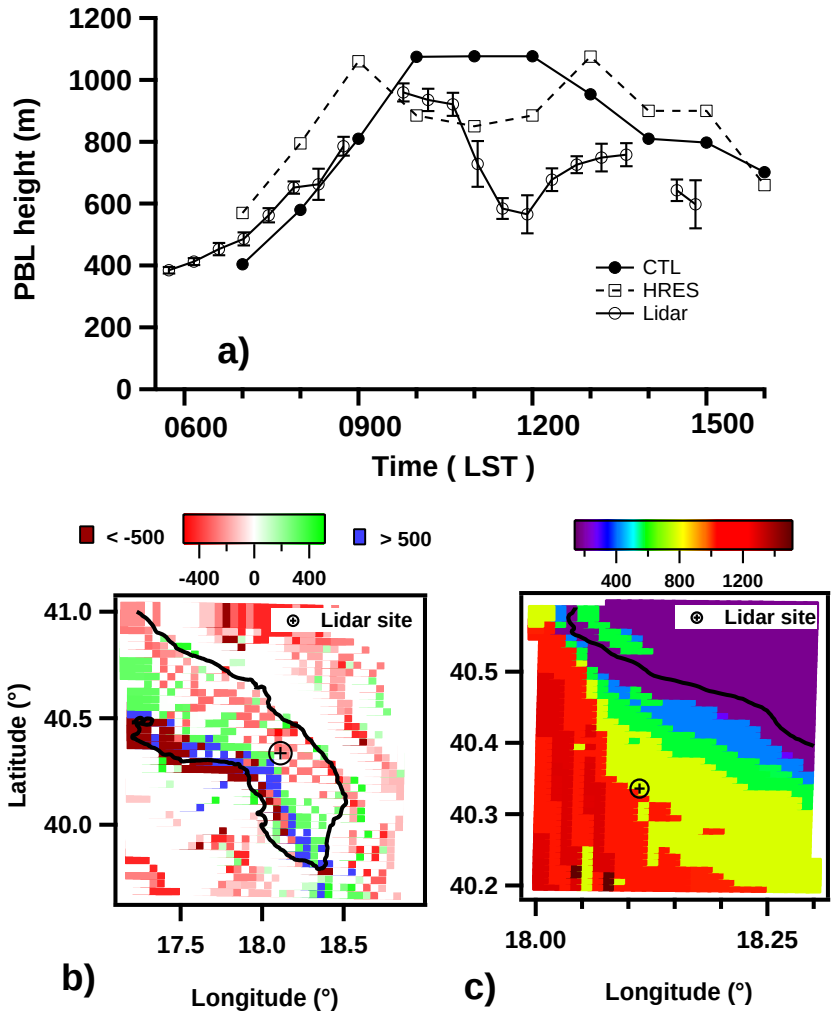

Fig. 5 a) The evolution of the PBL height in the lidar site, as calculated in the CTL run (full circles) and in the HRES run (squares), grid 2 of the WRF model, compared to the experimental results (open circles). The experimental measurement is obtained averaging over 30 minutes the altitudes corresponding to the maximum of fluctuations in Fig. 3. Error bars are the standard deviations of the samples. b) Plot of the difference between the PBL height at 1100 LST and 1300 LST as obtained by the CTL run, grid 2; c) PBL height at 1100 LST, HRES run, grid 3. Only the region around the lidar site is shown.

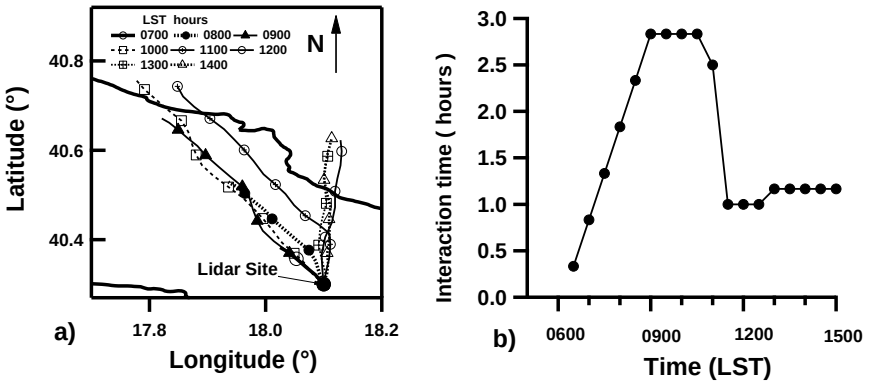

Fig. 6 a) Backtrajectories calculated from wind intensity and direction in Fig. 3a) at different day hours. Markers are spaced by 30 minutes. b) Interaction time (see text for details) as calculated from the backtrajectories.

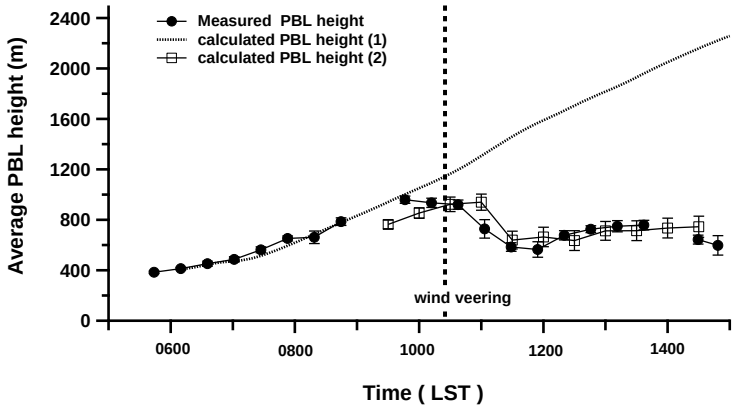

Fig. 7 Comparison between the measured and calculated PBL height. The experimental results are obtained as in Fig. 5. The theoretical values (dotted line and squares) have been obtained integrating Eq.12 for the time specified in Fig. 6b. After 0930 the dotted line represents the PBL height obtained not considering the formation of the internal boundary-layer. The error bars are the result of a sensitivity study as explained in the text.